Bull. Mater. Sci., Vol. 39, No. 4, August 2016, pp. 1091–1100. © Indian Academy of Sciences.
DOI 10.1007/s12034-016-1260-5

Electrospun chitosan/baker's yeast nanofibre adsorbent: preparation, characterization and application in heavy metal adsorption

MASUME HOSSEINI[1], ALI REZA KESHTKAR[2,*] and MOHAMMAD ALI MOOSAVIAN[1]
[1]Department of Chemical Engineering, Faculty of Engineering, University of Tehran, Tehran, Iran
[2]Nuclear Fuel Cycle School, Nuclear Science and Technology Research Institute, Tehran, Iran

MS received 22 May 2015; accepted 11 February 2016

Abstract. **In this study, chitosan/baker's yeast nanofibre was synthesized by electrospinning method and subsequently, the performance of the prepared nanofibre for removal of uranium(VI) and thorium(IV) ions from aqueous solutions was investigated. The prepared adsorbent was characterized by Brunauer–Emmett–Teller (BET), Fourier transform infrared spectroscopy (FTIR) and X-ray diffraction (XRD) analyses. The influences of experimental parameters on the chitosan/baker's yeast nanofibre such as contact time, pH, temperature and initial concentration were studied in a batch system. The adsorption kinetics was studied by the pseudo-first-order, pseudo-second-order, double-exponential and intra-particle kinetic models. Three isotherm models, namely Langmuir, Freundlich and Dubinin–Radushkevich (D–R) were used for analysis of equilibrium data of heavy metals. The maximum adsorption capacities of U(VI) and Th(IV) were estimated by Langmuir model to be 219 and 131.9 mg g^{-1} at optimum conditions, respectively. The positive values of the enthalpy changes and negative values of Gibbs free energy changes showed that U(VI) and Th(IV) adsorption process was endothermic and spontaneous. Also, the inhibitory effect of Co(II), Cu(II), Cd(II), Fe(II) and Ni(II) metal ions on U(VI) and Th(IV) adsorption was investigated. The reusability of chitosan/baker's yeast nanofibre was determined after five adsorption–desorption cycles.**

Keywords. **Electrospinning; chitosan/baker's yeast; nanofibre; heavy metal; adsorption.**

1. Introduction

Pollution by toxic heavy metals even at low concentrations is a serious danger to aquatic ecosystems. Considering that heavy metals are not biodegradable and accumulate in living organisms, they could harm human and animals in their natural environments [1]. Surface and ground waters have been contaminated by different ways, e.g., by industries which discharge contaminated waste into water resources without treatment. Since, it is necessary to remove the heavy metals, different methods and technologies are usually applied. These methods include adsorption, ion exchange, precipitation, evaporation, complexation, reverse osmosis and membrane processes [2–4]. Among them, adsorption method has been extensively used for removal of heavy and radioactive metal ions because this method is low-cost, environmentally compatible and very effective [5]. Electrospinning technique is an appropriate method for production of nanofibre adsorbents. Fibres prepared by electrospinning have high porosity and large surface area to improve adsorption capacity [6].

Application of biopolymers such as chitosan can be a low-cost method for the removal of pollutants from industrial wastewater. Chitosan is also an excellent adsorbent for heavy metals [7] because it has extraordinary properties such as biodegradability, abundance, hydrophilicity, non-toxicity and proper adsorption properties [8]. Chitosan applications are limited because it is soluble in acidic solutions. Crosslinking with epichlorohydrin, tripolyphosphate, ethylene glycol diglycidyl ether and glutaraldehyde has been used to modify chitosan chemically and prevent it from dissolving in acidic solutions, although it can decrease its adsorption capacity [8]. The metal adsorption capacity of chitosan varies with affinity for water, crystallinity, deacetylation degree and amino group content. Also, metal ion adsorption onto the chitosan differs depending on the raw material (shrimp, crab), preparation method, chemical modification and chitosan particle shape. On the other hand, baker's yeast is one of the most intensively studied biosorbents due to its wide use in the fermentation industry. Many studies have shown the capability of baker's yeast (*Saccharomyces cerevisiae*) for heavy metals removal, but less efforts are dedicated for application of immobilized biosorbents [9].

Recently, baker's yeast was exhibited to be an effective adsorbent for removal of nickel(II) [10], cadmium(II) [11,12], Lead(II) [12] and copper [13].

Radioactive waste originates from the nuclear industrial activities and some human activities such as exploitation of uranium and thorium ores. The removal of U(VI) and Th(IV) is a major purpose for industry and saving clean water resources. Nuclear industrial effluent contains many other heavy metal ions such as Fe(II), Cu(II), Ni(II), Cd(II) and Co(II), which may interfere with the adsorption process of

*Author for correspondence (akeshtkar@aeoi.org.ir)

U(VI) and Th(IV) ions [14,15]. In recent years, different adsorbents were used for U(VI) and Th(IV) removal from industrial effluent. However, due to the large number of candidate adsorbents, adsorption of U(VI) and Th(IV) ions needs to be deepened and more adsorbents need to be tested. For many heavy metal ions, chitosan and baker's yeast adsorbents have shown excellent binding capacity [9–16], which is even higher than that of the commercial adsorbents. Saifuddin and Raziah [17] studied Cr(VI) removal from aqueous solutions by *S. cerevisiae* immobilized in chitosan beads in a batch and continuous mode. Their results showed that the maximum biosorption capacity of encapsulated yeast cells in chitosan/lignosulphonate (as crosslinked agent) matrix is 86.95 mg g^{-1}. However, the adsorption potential of electrospun chitosan/baker's yeast nanofibre adsorbent towards heavy metals ions has not been investigated yet. Therefore, in this study, a novel chitosan/baker's yeast nanofibre adsorbent was synthesized by electrospinning method and its properties were characterized by Brunauer–Emmett–Teller (BET), Fourier transform infrared spectroscopy (FTIR) and X-ray diffraction (XRD) analyses. Also, the stability of nanofibre adsorbent was chemically improved by glutaraldehyde vapour. The objective of this paper is to investigate the adsorption potential of chitosan/baker's yeast nanofibre adsorbent for U(VI) and Th(IV) removal from aqueous solutions.

2. Experimental

2.1 *Materials*

Chitosan (75–85% deacetylated) with medium molecular weight and glutaraldehyde solution (25 wt%) were supplied by Sigma-Aldrich. The baker's yeast was obtained from Iranmellas Co, Iran. Trifluoroaceticacid 99% (TFA), $UO_2(NO_3)_2 \cdot 6H_2O$ and $Th(NO_3)_4 \cdot 4H_2O$ were purchased from Merck, Germany. HCl and NaCl were used to control the pH of the metal solutions. The standard solutions (1000 mg l^{-1}) were prepared by dissolving salts in distilled water.

2.2 *Preparation of chitosan/baker's yeast nanofibre*

For preparation of a 3% (w/v) chitosan solution, the weighed amount of chitosan powder was dissolved in 99% TFA (100 ml). After 24 h stirring at 25°C by a magnetic stirrer, baker's yeast was added into the solution with ratio of 6 : 1 and stirred for 48 h. Finally, the prepared solution was homogenized with ultrasonic vibration for 2 h.

The homogenized solution was loaded into a 10 ml plastic syringe with a 0.5 mm capillary tip diameter. After transferring the syringe to electrospinning box, a voltage of 15–18 kV with a tip-collector distance of 20 cm and a flow rate of 0.5 ml h^{-1} were applied to the solution and the fibres were collected on the cylindrical collector as fibrous membrane.

To increase the stability, the composite nanofibre was put in a chamber consisting of vapour phase of glutaraldehyde 25% for 10 h. Finally, the nanofibre was dried for 24 h.

2.3 *Characterization*

The functional groups of prepared nanofibre were determined by FTIR (Vector22-Bruker Company, Germany) in the range of 4000–400 cm^{-1}. Specific surface areas and pore diameter of nanofibre were measured with BET (Covanto crom-Nova 2000 Company, America) method. XRD (Stidy-mp Company, Germany) patterns were carried out to determine the characteristic of the crystalline peaks at around $2\theta = 10$–$80°$.

2.4 *Batch experiments*

All experiments were conducted in 250 ml Erlenmeyer flasks by adding 50 mg of chitosan/baker's yeast nanofibre to 50 ml of U(VI) or Th(IV) solutions with an initial ion concentration of 100 mg l^{-1}. The solutions were placed at a constant temperature of 25°C on a rotary shaker at 150 rpm for 180 min. The pH of each solution was adjusted using 0.1 mol l^{-1} NaOH and/or 0.1 mol l^{-1} HCl solution. Consequently, the filtered liquid was analysed to determine the concentration of U(VI) and Th(IV) ions using an inductively coupled plasma emission spectrometer (ICP-AES) (Thermo Jarrel Ash, Model Trace Scan).

The adsorption capacity at equilibrium (q_e, mg g^{-1}) was calculated as follows:

$$q_e = \frac{(C_0 - C_e)\, V}{W}, \tag{1}$$

where C_0 and C_e are the initial and equilibrium concentrations of metal solutions (mg l^{-1}), V the volume of aqueous solution (l) and W the mass of chitosan/baker's yeast nanofibre (g).

3. Results and discussion

3.1 *Characterization of chitosan/baker's yeast nanofibre*

XRD image of nanofibre adsorbent is shown in figure 1. As can be seen, there is an obvious peak at $2\theta = 10.54°$, which is ascribed to low crystallinity of nanofibre adsorbent. Changes in peak positions of FTIR spectra of the chitosan/baker's yeast nanofibre before and after adsorption of U(VI) and Th(IV) are shown in figure 2. The broad band in the range of 3200–3600 cm^{-1} is attributed to O–H and N–H stretching of the polysaccharide molecules [18]. The bands in the regions of 1674 and 1531 cm^{-1}, 896 and 1194 cm^{-1} and 2936 and 1050 cm^{-1} were assigned to NH_2 and NH, saccharide structure and –CH [19] and CO in the structure of the chitosan/baker's yeast nanofibre [20], respectively. After adsorption of U(VI), the peaks of NH_2, NH, –CH and CO groups shifted to 1672, 1530, 2935 and 1042 cm^{-1}, respectively. The peak changes also occurred after adsorption of Th(IV), so that NH_2, –CH and CO groups shifted to 1670, 2930 and 1022 cm^{-1}, respectively, in addition to the appearance of a very weak NH bending band. Also, the peak of the 1094 cm^{-1} related to phosphodiester group ($-PO_2^-$) after adsorption of

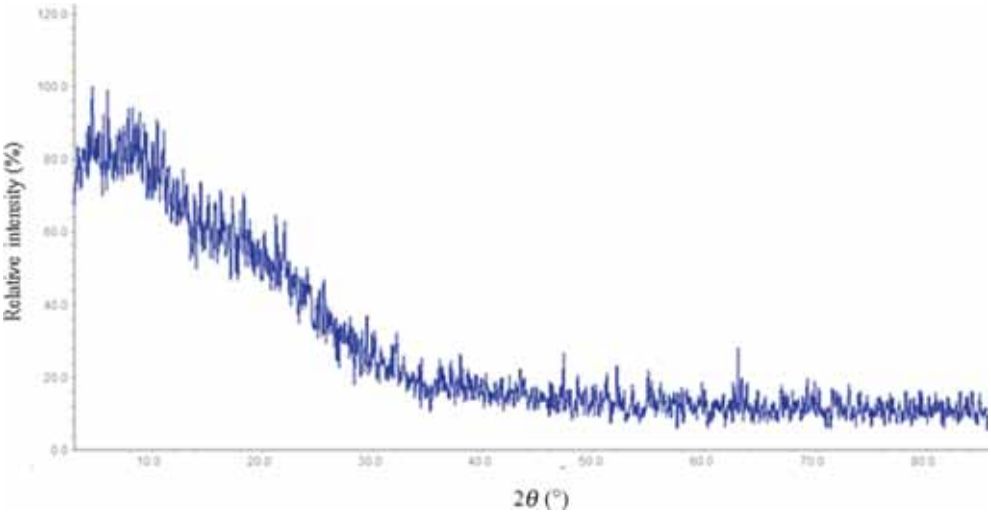

Figure 1. XRD pattern for chitosan/baker's yeast nanofibre.

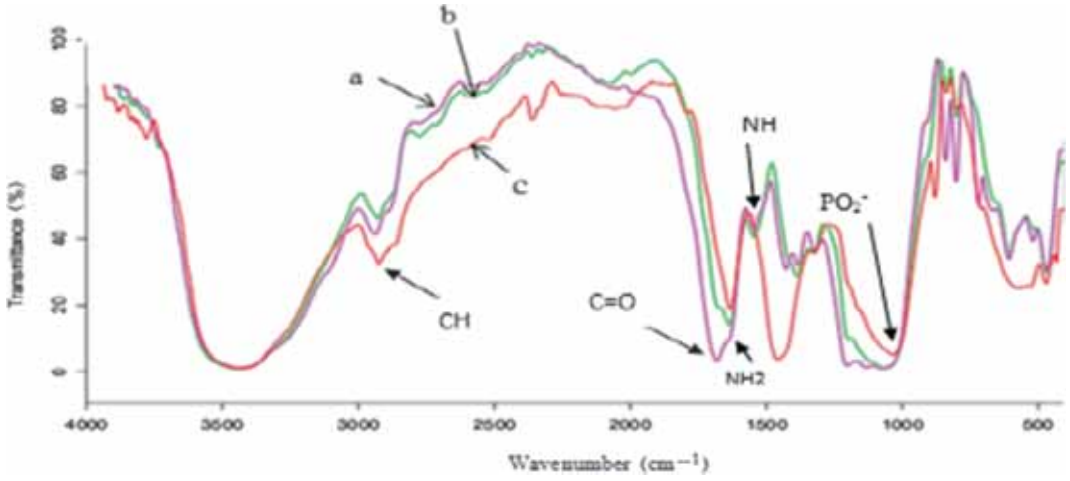

Figure 2. FTIR spectra of (**a**) chitosan/baker's yeast nanofibre, (**b**) after adsorption of uranium(VI) and (**c**) thorium(IV).

U(VI) and Th(IV) disappeared [21], and the peak of carboxyl groups (C=O) shifted from 1648 to 1637 cm^{-1} and 1641 cm^{-1}, respectively [16]. This showed that the oxygen atoms of carboxyl groups and metal ions were coordinated to guide the shifting of carboxyl groups [22]. Comparison of FTIR spectra before and after adsorption showed no other important peak changes. So, phosphodiester, carboxyl, methyl and amine groups of this nanofibre play a great role in U(VI) and Th(IV) adsorption.

The nitrogen adsorption–desorption isotherm for the chitosan/baker's yeast nanofibre is shown in figure 3a. Based on BJH theory, the average pore diameter, the surface area and the pore volume of these nanofibres were 1.946 nm, 8.454 m^2 g^{-1} and 0.031 cm^3 g^{-1}, respectively. The highest and the lowest adsorption and desorption points of chitosan/baker's yeast nanofibre were obtained at p/p_0 of approximately 0.90 and 0.05, respectively. The pore size distribution of chitosan/baker's yeast nanofibre is shown in figure 3b. The value of pore diameter showed that the surface of chitosan/baker's yeast nanofibre was mesoporous.

3.2 *Effect of pH*

The adsorption of U(VI) and Th(IV) onto the chitosan/baker's yeast nanofibre in different initial pH values was tested to explain the effect of solution pH on adsorption capacity because it is a significant operational parameter in the adsorption process. Adsorption capacity for U(VI) and Th(IV) is shown in figure 4.

Figure 4 shows that the maximum adsorption capacity occurs at pH 6.0 for U(VI) and Th(IV). It can be seen that the adsorption capacities increased as an increase in pH. As can be seen in figure 4, there is a low adsorption of U(VI) and Th(IV) at initial pH values, because the active sites of nanofibre adsorbent were mainly protonated. As pH values increases, the available sites on the nanofibre adsorbent for

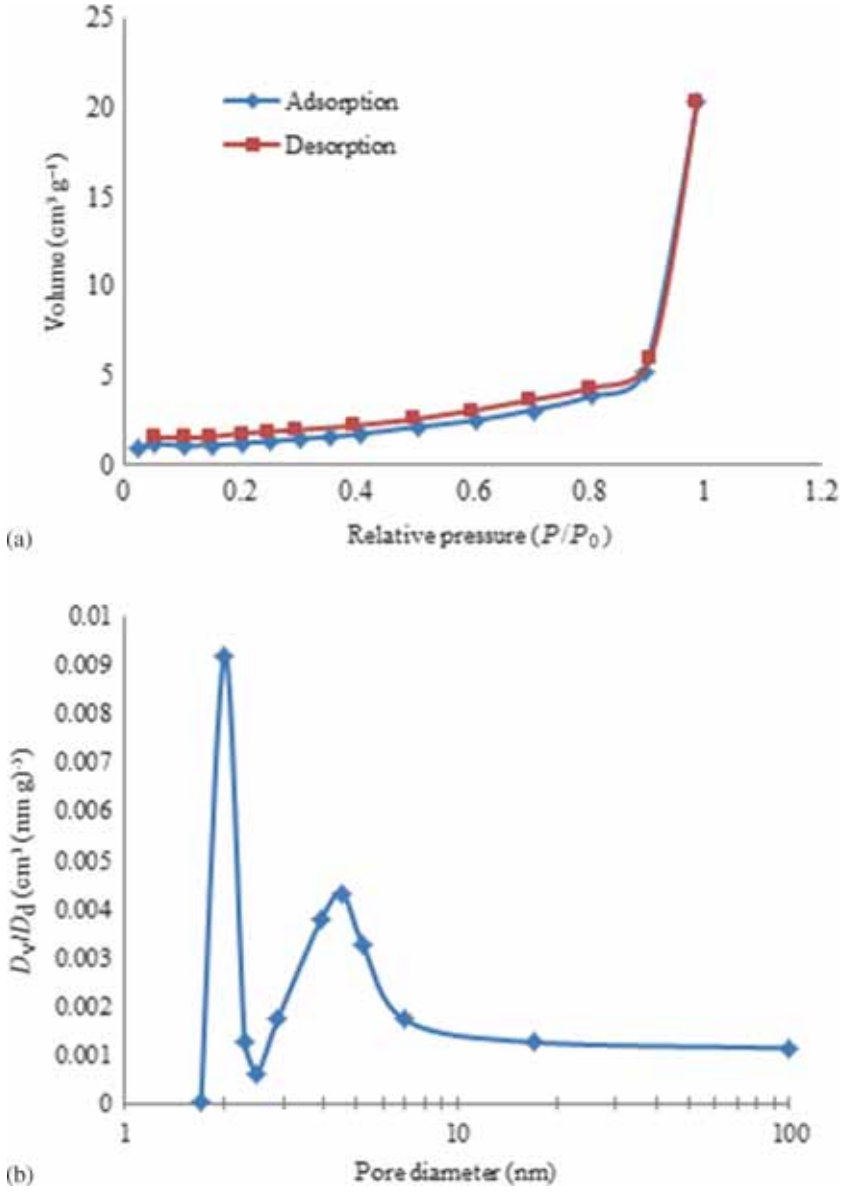

Figure 3. (**a**) Nitrogen adsorption–desorption isotherm and (**b**) the pore size distribution by BJH method of chitosan/baker's yeast nanofibre.

cations reach the maximum at pH 6. The metal species in solution were calculated at pH 6 and initial metal ion concentration of 100 mg l^{-1} using the Visual Minteq software. The results showed that the various hydrate complexes with different charges and sizes, mainly $Th(OH)_2^{2+}$, $Th(OH)^{3+}$, UO_2OH^+, $(UO_2)_3(OH)_5^+$, $(UO_2)_4(OH)_7^+$ and $(UO_2)_2(OH)_2^{2+}$, were present in the solution.

3.3 *Effect of contact time*

The effect of contact time on U(VI) and Th(IV) adsorption was studied at initial metal ions concentration of 100 mg l^{-1}, adsorbent dosage of 1 g l^{-1} and temperature of 25°C within the time range of 30–120 min. The results showed that the adsorption onto the chitosan/baker's yeast nanofibre reached the equilibrium after about 180 min. The metal ions removal rate was initially fast because of a large number of vacant adsorption sites on the adsorbent surface. The results showed that more than 77.86 and 92.87% of U(VI) and Th(IV) were adsorbed onto the nanofibre adsorbent during the initial contact time of 90 min and then, the adsorption capacity values of metal ions slowly approached to its equilibrium states. The adsorption capacity of U(VI) and Th(IV) at equilibrium state was found to be 57.86 and 33.70 mg g^{-1}, respectively.

3.4 *Effect of initial metal ions concentration and temperature*

The initial metal ions concentration and temperature are very significant parameters. The effect of these parameters on U(VI) and Th(IV) adsorption was studied at adsorbent

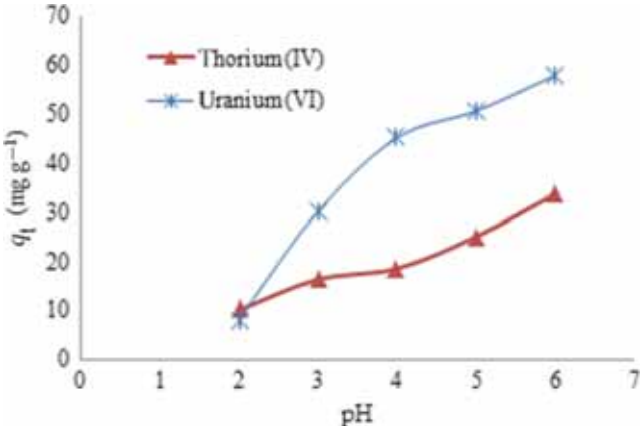

Figure 4. Effect of pH on the desorption of uranium(VI) and thorium(IV) by chitosan/baker's yeast nanofibre. Initial metal ions concentration = 100 mg l^{-1}, adsorbent dosage = 1 g l^{-1} and temperature = 25°C.

dosage of 1 g l^{-1}, pH 6, initial metal ion concentrations ranging from 50 to 500 mg l^{-1} and different temperatures from 25 to 45°C. The results of equilibrium adsorption capacity of U(VI) and Th(IV) are given in figure 5. As can be seen, the adsorption capacity of nanofibre adsorbent increases with an increase in initial metal ions concentration. Also, the experimental results show that the adsorption capacity of both metal ions increases as the temperature rises. These data approve that the adsorption process of U(VI) and Th(IV) metal ions onto the chitosan/baker's yeast nanofibre is endothermic.

3.5 *Equilibrium adsorption isotherm*

The adsorbed metal ions onto the chitosan/baker's yeast were expressed by isotherm models at equilibrium concentration of metal ions. In the present study, Langmuir, Freundlich and Dubin–Radushkevich (D–R) isotherms equations were used to model the equilibrium adsorption of U(VI) and Th(IV) metal ions onto the chitosan/baker's yeast nanofibre at three temperatures of 25, 35 and 45°C.

Langmuir model assumes that the adsorption energy is distributed homogeneously over the entire coverage and there is no interaction between adsorbed molecules. Also, it assumes that the monolayer sorption occurs when the molecules adsorb on fixed positions on the surface of the adsorbent. The nonlinear form of this model is shown by the following equation [23]:

$$q_e = \frac{q_m K_L C_e}{1 + K_L C_e}, \tag{2}$$

where q_e (mg g^{-1}) is the equilibrium metal ions adsorption onto the nanofibre, C_e (mg l^{-1}) the equilibrium metal ions concentration, q_m the maximum monolayer adsorption capacity and K_L (l mg^{-1}) a constant. The higher value of K_L indicates intensive adsorption bonding of metal ions onto the nanofibre adsorbent.

One of the essential parameters of the Langmuir model is the separation factor (R_L), which is explained by the following equation [24]:

$$R_L = \frac{1}{1 + K_L C_0}, \tag{3}$$

where K_L (l mg^{-1}) is Langmuir constant and C_0 (mg l^{-1}) the maximum initial concentration. The value of R_L indicates the favourable or unfavourable types of the adsorption isotherm.

Freundlich model is one of the earliest experimental models used to explain the equilibrium data. This Freundlich isotherm expresses multilayer adsorption on a heterogeneous surface. The nonlinear form of this model is given as follows [25]:

$$q_e = K_F C_e^n, \tag{4}$$

where K_F and n are Freundlich constants representing the adsorption capacity and intensity of the adsorbent, respectively.

Dubin–Radushkevich (D–R) isotherm model is used to determine the nature of adsorption processes as physical or chemical. The nonlinear form of D–R isotherm equation is shown as follows [26]:

$$q_e = q_{DR} \exp\left(-\beta_{DR} \varepsilon^2\right), \tag{5}$$

where q_e (mmol g^{-1}) is the value of metal ions adsorbed onto the adsorbent, q_{DR} (mmol g^{-1}) the maximum adsorption capacity, β (mol^2 kJ^{-2}) a constant related to the mean free energy of adsorption per mole of the adsorbate and the mean free energy of adsorption could be calculated according to $E = 1/\sqrt{2\beta}$ equation and gives information about physical and chemical mechanisms. If E-value lies between 8 and 16 kJ mol^{-1}, the adsorption mechanism occurs chemically and if E-value is lower than 8 kJ mol^{-1}, the adsorption mechanism occurs physically [27]. ε is the Polanyi potential, which is related to equilibrium concentration and can be expressed as follows:

$$\varepsilon = RT \ln\left(1 + \frac{1}{c_e}\right), \tag{6}$$

where R (8.314 J mol^{-1} K^{-1}) is the gas constant and T the absolute temperature. The parameters of Langmuir, Freundlich and Dubinin–Radushkevich (D–R) isotherm models and regression coefficients (R^2-values) were obtained from nonlinear regression of equilibrium data using the MATLAB software and the results are given in table 1. By comparing the R^2-values of all isotherms, experimental data of the adsorption of U(VI) and Th(IV) metal ions onto the chitosan/baker's yeast nanofibre at three temperatures fitted well with Langmuir isotherm model. The maximum adsorption capacity based on Langmuir model increased with a rise in temperature. As can be seen in table 1, the q_m values were found to be 202.9, 206.2 and 219.0 mg g^{-1} for U(VI) adsorption and 122.8, 124.5 and 131.9 mg g^{-1} for Th(IV) adsorption at temperatures of 25, 35 and 45°C, respectively. Also, R_L values of chitosan/baker's yeast nanofibre were between 0 and 1,

indicating favourable adsorption process of both metal ions at all studied temperatures. The E-values obtained from D–R model were 3.285, 3.773, 4.708 kJ mol^{-1} for U(VI) and 2.751, 3.186, 3.771 kJ mol^{-1} for Th(IV), at temperature of 25, 35 and 45°C, respectively. The adsorption of these heavy metal ions onto the chitosan/baker's yeast nanofibre shows that this process is a physical process.

3.6 *Adsorption kinetics*

Kinetic data of process are needed to design adsorption units. Metal ions adsorption kinetics is controlled by the adsorption reaction rates and the mass transfer rates in aqueous and solid phases. Three sequential stages of the adsorption by a porous adsorbent are solute mass transfer into the external

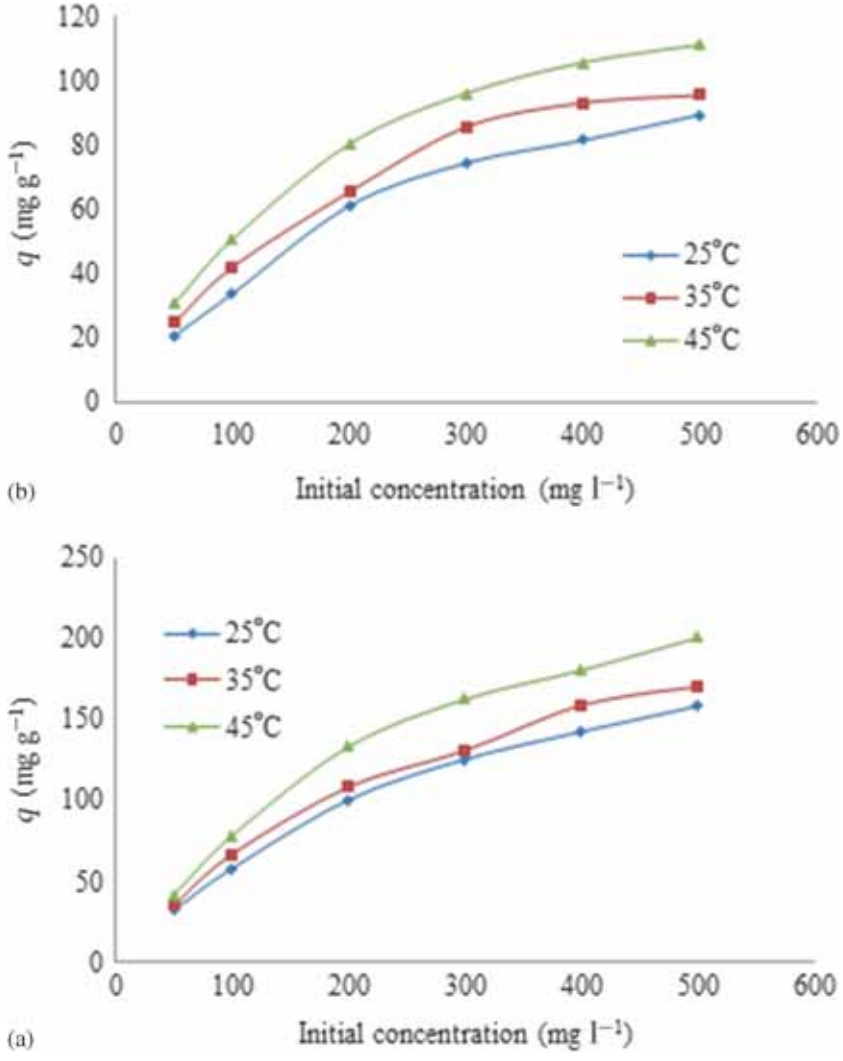

Figure 5. Effect of (**a**) initial uranium(VI) and (**b**) thorium(IV) concentrations and temperature on the adsorption capacity. Adsorbent dosage = 1 g l^{-1} and pH = 6.

Table 1. Adsorption isotherms parameters for adsorption of uranium(VI) and thorium(IV).

		Langmuir				Freundlich			D–R			
Metal ion	T (°C)	q_m (mg g^{-1})	K_L (l mg^{-1})	R_L	R^2	K_F (mg g^{-1})	n	R^2	q_{DR} (mmol g^{-1})	B_{DR} (mol^2 kJ^{-2})	E (kJ mol^{-1})	R^2
U(VI)	25	202.9	0.00960	0.1724	0.9983	10.43	0.4717	0.9811	0.68	4.633E−8	3.285	0.9795
	35	206.2	0.01259	0.1371	0.9883	13.75	0.4401	0.9835	0.72	3.514E−8	3.773	0.9671
	45	219.0	0.02393	0.0771	0.9928	25.24	0.3671	0.9730	0.84	2.255E−8	4.708	0.9847
Th(IV)	25	122.8	0.00650	0.2352	0.9940	4.67	0.4975	0.9675	0.40	6.605E−8	2.751	0.9784
	35	124.5	0.00898	0.1822	0.9928	7.23	0.4416	0.9620	0.43	4.925E−8	3.186	0.9744
	45	131.9	0.01327	0.1309	0.9972	11.50	0.3887	0.9729	0.49	3.516E−8	3.771	0.9781

liquid film, diffusion of the solute into the pores of adsorbent and the solute adsorption onto the external and internal surfaces of the adsorbent [28].

In this study, the pseudo-first-order, pseudo-second-order, intra-particle diffusion and double-exponential models were used to depict the adsorption kinetics of U(VI) and Th(IV) onto the chitosan/baker's yeast nanofibre adsorbent.

The equation of the pseudo-first-order model is given as [16]:

$$q_t = q_e \left(1 - \exp\left(-k_1 t\right)\right), \tag{7}$$

where q_e (mg g^{-1}) and q_t (mg g^{-1}) are the adsorption capacities at equilibrium and time t, respectively, and k_1 (min^{-1}) is pseudo-first-order adsorption rate constant.

The nonlinear form of the pseudo-second-order kinetics is given as [29]:

$$q_t = \frac{k_2 q_e^2 t}{1 + k_2 q_e t}, \tag{8}$$

where k_2 (g (mg min)$^{-1}$) is the pseudo-second-order rate constant of adsorption. The intra-particle diffusion model has been used to inspect the internal diffusion behaviour of metal ions onto the nanofibre. In this model, the adsorption kinetics of metal ions is controlled by intra-particle diffusion [16]. This model can be explained as follows [30]:

$$q_t = k t^{0.5}, \tag{9}$$

where k (mg g^{-1} min$^{-0.5}$) is the intra-particle diffusion rate constant.

The double-exponential model explains a two-step mechanism of adsorption kinetics, a rapid step which is ascribed to the external diffusion of metal ions and a slow step which is attributed to the internal diffusion of metal ions onto the nanofibre adsorbent. This model is given as [31]:

$$q_t = q_e - \frac{D_1}{m_a}\exp\left(-K_{D_1} t\right) - \frac{D_2}{m_a}\exp\left(-K_{D_2} t\right), \tag{10}$$

where D_1 and D_2 are the adsorption rates (g l^{-1}) of the rapid and slow steps, respectively, and K_{D_1} and K_{D_2} (min^{-1}) are controlling constants of the mechanism and m_a is (g l^{-1}) the adsorbent dosage. The kinetic data of U(VI) and Th(IV) adsorption onto the chitosan/baker's yeast nanofibre adsorbent were described with four kinetic models and the nonlinear regression results using MATLAB software are given in table 2. By comparing the values of regression coefficients for kinetic models of both metal ions, it was found that the higher regression coefficient belonged to the double-exponential and the experimental data were best fitted this model. According to this model, it is concluded that the U(VI) and Th(IV) adsorption onto the chitosan/baker's yeast nanofibre adsorbent consists of two steps, the first step includes the external diffusion (rapid step) and second step includes the pore diffusion (slow phase).

3.7 *Adsorption thermodynamic*

The experimental information achieved at three temperatures were used for estimating the thermodynamic parameters, including Gibbs free energy change (ΔG°), enthalpy change (ΔH°) and entropy change (ΔS°). Thermodynamic parameters show the nature of adsorption. The Gibbs free energy is calculated by the following equations [32]:

$$\Delta G^\circ = -RT \ln k_c, \tag{11}$$

$$k_c = \lim_{C_{el}\to 0} \frac{C_{es}}{C_{el}}, \tag{12}$$

where R is gas constant (8.314 J mol^{-1} K^{-1}), T the temperature (K) and k_c the equilibrium constant. C_{es} (mg l^{-1}) is solid phase equilibrium concentration and C_{el} (mg l^{-1}) the liquid phase equilibrium concentration. ΔH° and ΔS° were calculated with the following equation [33]:

$$\ln k_c = \frac{\Delta S^\circ}{R} - \frac{\Delta H^\circ}{RT}, \tag{13}$$

Table 2. Kinetic parameters of uranium(VI) and thorium(IV) adsorption onto the chitosan/baker's yeast nanofibre.

Metal ion	q_e (mg g^{-1})						
				Pseudo-first-order			
		k_1 (min)$^{-1}$		q (mg g^{-1})			R^2
U(VI)	57.86	0.01287		62.79			0.9983
Th(IV)	33.70	0.03943		32.93			0.9245
				Pseudo-second-order			
		k_2 (g (mg min))$^{-1}$		q (mg g^{-1})			R^2
U(VI)	57.86	0.000126		85.64			0.9922
Th(IV)	33.70	0.001751		36.31			0.9948
				Intra-particle			
		k (mg g^{-1} min$^{-0.5}$)					R^2
U(VI)	57.86	4.229					0.9604
Th(IV)	33.70	1.039					0.9174
				Double-exponential			
		D_1 (g l^{-1})	K_{D_1} (min)$^{-1}$	D_2 (g l^{-1})	K_{D_2} (min)$^{-1}$	q_e (mg g^{-1})	R^2
U(VI)	57.86	65.40	0.0145	0.95	0.921	61.34	0.9997
Th(IV)	33.70	18.10	0.0197	0.42	0.784	33.92	0.9990

Table 3. Thermodynamic parameters for metal ions adsorption onto the chitosan/baker's yeast nanofibre.

Metal ion	k_c			ΔH°	ΔS°	ΔG° (kJ mol^{-1})		
	25°C	35°C	45°C	(kJ mol^{-1})	(kJ (mol k)$^{-1}$)	25°C	35°C	45°C
U(VI)	1.91	2.20	3.61	24.090	0.0885	−1.6041	−2.0200	−3.3951
Th(IV)	1.03	1.21	1.62	17.795	0.0599	−0.0733	−0.4884	−1.2761

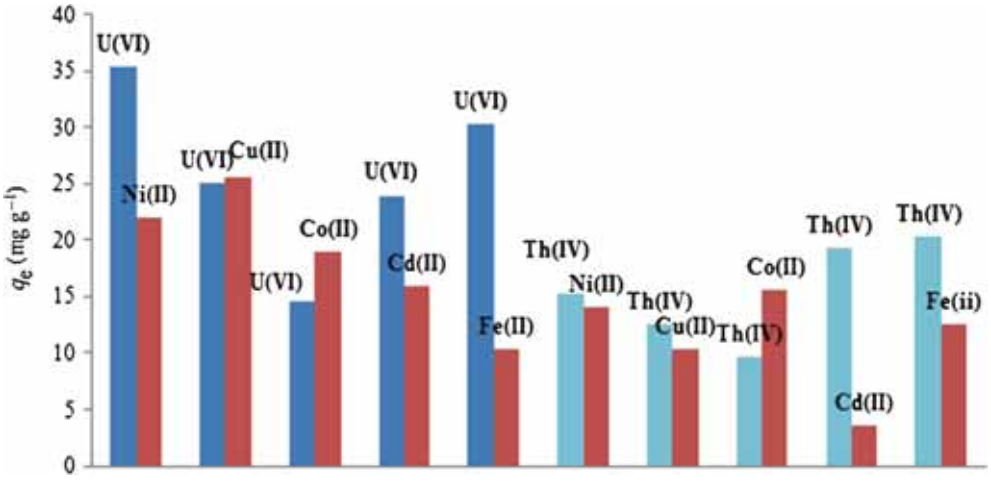

Figure 6. Adsorption capacity of uranium(VI) and thorium(IV) in binary systems.

where $\Delta H^\circ/R$ and $\Delta S^\circ/R$ are obtained from the slope and intercept of $\ln k_c$ *vs.* $1/T$ plot. The calculated thermodynamic parameters of heavy metals are shown in table 3. As shown in table 3, the ΔG° values are negative for U(VI) and Th(IV) under all studied conditions. This shows the feasibility and spontaneity of U(VI) and Th(IV) adsorption by the chitosan/baker's yeast nanofibre. In addition, the value of ΔG° decreased with an increase in temperature which indicates that the higher temperature is more favourable for the adsorption of U(VI) and Th(IV) ions.

The positive values of ΔH° showed the endothermic nature of heavy metals adsorption onto the nanofibre. The enthalpy changes were 25.04 and 17.30 KJ mol^{-1} for U(VI) and Th(IV), respectively, which confirms that the adsorption was a physical process [34].

The positive ΔS° values of two heavy metal ions proved the increased randomness of the chitosan/baker's yeast nanofibre-solution interface during the adsorption [35].

Metal adsorption can take place either by electrostatic interaction, ion exchange, surface complexation, precipitation or combination of these interactions. Presence of various functional groups such as phosphodiester, hydroxyl, amine and carboxyl within the structure of nanofibre adsorbent shows the fact that the mechanism of adsorption will not be restricted to physical interaction. The amine and hydroxyl groups on the chitosan after and before crosslinking act as chelation sites [36]. In addition, due to surface properties of baker's yeast, electrostatic attraction to negatively charged functional groups may be one of the mechanisms [37]. So, the adsorption of U(VI) and Th(IV) on the nanofibre adsorbent can take place by combination of electrostatic interaction and surface complexation.

3.8 *Inhibitory effect of other metal ions*

The metal ion adsorption capacity is often reduced by the presence of other metal ions in aqueous solutions [2,38,39]. To investigate this inhibitory effect on U(VI) and Th(IV) adsorption onto the chitosan/baker's yeast nanofibre, the experiments were conducted in binary solutions consisting of 100 mg l^{-1} U(VI) and Th(IV) and 50 mg l^{-1} other metal ions such as Cu(II), Co(II), Cd(II), Fe(II) and Ni(II) at pH 6 and temperature of 25°C. The results of adsorbed amount of each metal ion onto the adsorbent are shown in figure 6. As can be seen, the adsorption capacity of U(VI) and Th(IV) ions decreased in binary systems and the inhibitory effect of these metal ions on the U(VI) and Th(IV) adsorption was in the order of Co(II) > Cd(II) > Cu(II) > Fe(II) > Ni(II) and Co(II) > Cu(II) > Ni(II) > Cd(II) > Fe(II), respectively. Also, the results showed that the Th(IV) adsorption onto the chitosan/baker's yeast nanofibre was inhibited more than U(VI) adsorption in binary systems. As illustrated in figure 6, the nanofibre adsorbent had a complex affinity with different heavy metal ions due to the properties of the adsorbent functional groups and metal sorbate. Several researchers attempted to correlate these differences in metal adsorption with the properties of metal ions such as ionic radii, atomic weight and electronegativity of the metal [40,41]. However, no correlation can be made in the present study as the competition between the metal ions in binary systems also plays

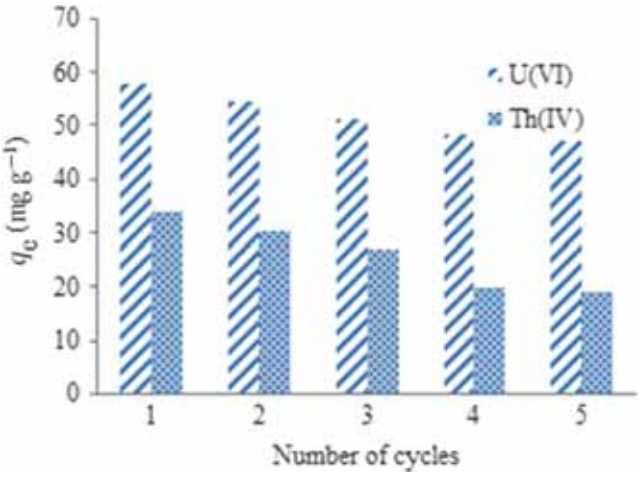

Figure 7. Adsorption–desorption cycles for chitosan/baker's yeast nanofibre.

a significant role in addition to the affinity of each metal ion with binding site.

3.9 *Desorption of chitosan/baker's yeast nanofibre*

Desorption studies of the adsorbent and regeneration capacity are necessary factors in the adsorption process because reusability of the adsorbent is a key factor in improving economic process. Adsorption process was performed at pH 6, adsorbent dosage of 1 g l^{-1}, contact time of 180 min, temperature of 25°C and initial uranium(VI) or thorium(IV) concentrations of 100 mg l^{-1}. After adsorption experiment, the chitosan/baker's yeast nanofibre was immersed in 30 ml of elution solution and stirred at 150 rpm for 6 h. In this study, 0.1 M Na_2CO_3 and 0.1 M HNO_3 as suitable elution solutions were selected for regenerating process [25]. The reusability of the adsorbent was estimated in five adsorption–desorption cycles and the results of which are shown in figure 7. A slight decrease in adsorption capacity of metal ions after five cycles of adsorption–desorption might be attributed to the loss of adsorbents during the multiple washing steps after each adsorption–desorption cycle. In addition, it might be due to the losing of active sites of adsorbent after each desorption by elution solution. The results indicated that the nanofibre can be reused frequently without any significant loss in adsorption performance.

4. Conclusion

In this study, a new chitosan/baker's yeast nanofibre adsorbent was prepared for adsorption of U(VI) and Th(IV) ions from aqueous solutions by the electrospinning process. BET analysis showed that the average pore diameter, pore volume and the surface area were 1.946 nm, 0.031 cm^3 g^{-1} and 8.454 m^2 g^{-1}, respectively. XRD pattern of chitosan/baker's yeast nanofibre showed a low crystallinity. The effect of parameters such as pH, contact time and temperature was investigated on the adsorption of U(VI) and Th(IV) from aqueous solutions. Three isotherm models, namely Langmuir, Freundlich and Dubin–Radushkevich (D–R) were used for analysis of equilibrium data. The results showed that the Langmuir isotherm described the equilibrium data of U(VI) and Th(IV) adsorption better than the other isotherm models representing that the adsorption was monolayer and maximum adsorption capacities for U(VI) and Th(IV) were 219.0 and 131.9 mg g^{-1}, respectively, at the temperature of 45°C. The adsorption capacity of U(VI) and Th(IV) ions by the chitosan/baker's yeast nanofibre was in the order of (U(VI) > Th(IV)). The adsorption kinetic studies of both metal ions explained that the experimental data were best described by double-exponential one. The positive values of the enthalpy changes showed that U(VI) and Th(IV) adsorption processes were endothermic. Negative values of Gibbs free energy changes showed that the adsorption of these metal ions onto the chitosan/baker's yeast nanofibre adsorbent was spontaneous. The results of inhibitory effect of Co(II), Cd(II), Cu(II), Fe(II) and Ni(II) on the U(VI) and Th(IV) adsorption onto the chitosan/baker's yeast nanofibre showed that the adsorption capacity of U(VI) and Th(IV) ions decreased in binary systems, according to the descending order of Co(II) > Cd(II) > Cu(II) > Fe(II) > Ni(II) and Co(II) > Cu(II) > Ni(II) > Cd(II) > Fe(II) for U(VI) and Th(IV), respectively. The chitosan/baker's yeast nanofibre was regenerated with 0.1 M Na_2CO_3 and 0.1 M HNO_3 solution and no significant loss in the adsorption process of U(VI) and Th(IV) was observed after five adsorption–desorption cycles.

References

[1] Febrility J, Kosasih A N, Sunarso J, Ju Y, Indraswati N and Ismadji S 2009 *J. Hazard. Mater.* **162** 616

[2] Han R, Zou W, Wang Y and Zhu L 2007 *J. Environ. Radioact.* **93** 127

[3] Nilchi A, Dehaghan T S and Garmarodi S R 2013 *Desalination* **321** 67

[4] Xiong C, Pi L, Chen X, Yang L, Ma C and Zheng X 2013 *Carbohydr. Polym.* **98** 1222

[5] Gavrilescu M 2004 *Eng. Life Sci.* **4** 219

[6] Agarwal S, Greiner A and Wendorff 2013 *J. Prog. Polym. Sci.* **38** 963

[7] Ren Y, Abbood H A, He F, Peng H and Huang K 2013 *Chem. Eng. J.* **226** 300

[8] Laus R and De Favere V T 2011 *Bioresource Technol.* **102** 8769

[9] Wang J and Chen C 2006 *Biotechnol. Adv.* **24** 427

[10] Padmavathy V, Vasudevan P and Dhingra S C 2003 *Process Biochem.* **38** 1389

[11] Vasudevan P, Padmavathy V and Dhingra S C 2003 *Bioresource Technol.* **89** 281

[12] Goksungur Y, Uren S and Guvenc U 2005 *Bioresource Technol.* **96** 103

[13] Zhang Y, Liu W, Xu M, heng F and Zhao M 2010 *J. Hazard. Mater.* **178** 1085

[14] Keshtkar A R, Mohammadi M and Moosavian M A 2015 *J. Radioanal. Nucl. Chem.* **303** 363

[15] Cecal A, Humelnicu D, Rudic V, Cepoi L, Ganju D and Cojocari A 2012 *Bioresource Technol.* **118** 19

[16] Gerente C, Lee V K C, Cloirec P L and McKay G 2007 *Crit. Rev. Env. Sci. Technol.* **37** 41

[17] Saifuddin N and Raziah A Z 2007 *J. Appl. Sci. Res.* **3** 2091

[18] Paipitak K, Pornpra T, Mongkontalang P, Techitdheera W and Pecharapa W 2011 *Procedia Eng.* **8** 101

[19] Li Y, Qiu T and Xu X 2013 *Eur. Polym. J.* **49** 1487

[20] Kiechel M A and Schauer C L 2013 *Carbohydr. Polym.* **95** 123

[21] Liu M, Dong F, Yan X, Zeng W, Hou L and Pang X 2010 *Bioresource Technol.* **101** 8573

[22] Li T T, Liu Y G, Peng Q Q, Hu X J, Liao T, Wang H and Lu M 2013 *Chem. Eng. J.* **214** 189

[23] Aliabadi M, Irani M, Ismaeili J and Najafzadeh S 2014 *J. Taiwan Inst. Chem. Eng.* **45** 518

[24] Xiong L, Chen C, Chen Q and Ni J 2011 *J. Hazard. Mater.* **189** 741

[25] Humelnicu D, Dinu M V and Dragan E S 2011 *J. Hazard. Mater.* **185** 447

[26] Hritcu D, Humelnicu D, Dodi G and Popa M I 2012 *Carbohydr. Polym.* **87** 1185

[27] Irani M, Keshtkar A R and Mousavian M A 2011 *Chem. Eng. J.* **175** 251

[28] Hu X J, Wang J S, Liu Y G, Li X, Zeng G M and Bao Z L 2011 *J. Hazard. Mater.* **185** 306

[29] Ozacar M, Sengil I A and Turkmenler H 2008 *Chem. Eng. J.* **143** 32

[30] Futalan C M, Kan C C, Dalida M L, Hsien K J, Pascua C and Wan M W 2011 *Carbohydr. Polym.* **83** 528

[31] Abbasizadeh S, Keshtkar A R and Mousavian M A 2013 *Chem. Eng. J.* **220** 161

[32] Irani M, Keshtkar A and Moosavian M 2012 *Chem. Eng. J.* **200** 192

[33] Donia A M, Atia A A, Moussa E M, El-Sherif A M and El-Magied M O A 2009 *Hydrometallurgy* **95** 183

[34] Min M, Shen L, Hong G, Zhu M, Zhang Y and Wang X 2012 *Chem. Eng. J.* **197** 88

[35] Aliabadi M, Irani M, Ismaeili J, Piri H and Parnian M J 2013 *Chem. Eng. J.* **220** 237

[36] Ngah W W, Endud C S and Mayanar R 2002 *React. Funct. Polym.* **50** 181

[37] Jeon C and Holl W H 2003 *Water. Res.* **37** 4770

[38] Zhang Y, Liu W, Zhang L and Zhao M 2011 *Appl. Surf. Sci.* **257** 9809

[39] Xue X and Li F 2008 *Micropor. Mesopor. Mater.* **116** 116

[40] Hallaji H, Keshtkar A R and Moosavian M A 2015 *J. Taiwan Inst. Chem. Eng.* **46** 109

[41] Sengil I A and Ozacar M *J. Hazard. Mater.* **166** 1488